[INVITED] Novel optical biosensing technologies for detection of mycotoxins

A. Nabok, A.G. Al-Rubaye, A.M. Al-Jawdah, A. Tsargorodska, J.-L. Marty, G. Catanante, A. Szekacs, E. Takacs

[INVITED] Novel optical biosensing technologies for detection of mycotoxins

NABOK, Aleksey <http://orcid.org/0000-0002-9078-1757>, AL-RUBAYE, A.G., AL-JAWDAH, A.M, TSARGORODSKAYA, Anna, MARTY, J.-L., CATANANTE, G., SZEKACS, A. and TAKACS, E.

Published version

NABOK, Aleksey, AL-RUBAYE, A.G., AL-JAWDAH, A.M, TSARGORODSKAYA, Anna, MARTY, J.-L., CATANANTE, G., SZEKACS, A. and TAKACS, E. (2019). [INVITED] Novel optical biosensing technologies for detection of mycotoxins. Optics & Laser Technology, 109, 212-221.

Novel optical biosensing technologies for detection of mycotoxins

A. Nabok[1*], A. G. Al-Rubaye[1], A. M. Al-Jawdah[1], A. Tsargorodska[1], J.-L. Marty[2], G. Catanante[2], A. Szekacs[3], E. Takacs[3]

[1] Sheffield Hallam University, Materials and Engineering Research Institute, UK

[2] Perpignan University, Department of Biochemistry and Molecular Biology, France

[3] Agro-Environmental Research Institute, NARIC, Budapest, Hungary

Abstract

This work reviews our recent progress in development of novel optical methods of detection of mycotoxins in direct assay with either specific antibodies or aptamers. The main method in this work was the total internal reflection ellipsometry (TIRE) combined with LSPR transducers based on gold nano-structures produced by annealing of thin gold films. The gold nano-islands produced were characterised with SEM, AFM, UV-visible absorption spectroscopy, and spectroscopic ellipsometry. The combination of TIRE and LSPR offers superior refractive index sensitivity as compared to traditional UV-vis absorption spectroscopy. The limitations of LSPR related to a short evanescent field decay length can be overcome using small-size bio-receptors, such as half-antibodies and aptamers. The achieved sensitivity of detection of mycotoxins in 0.01ppb level of concentration is sufficient for the use of this method for analysis of agriculture products, food and feed on the presence of mycotoxins. Even higher sensitivity in sub-ppt level was achieved with another optical biosensor developed recently; it is based on optical planar waveguide operating as polarization interferometer (PI). This method is promising for development of portable, highly sensitive, and simple to use biosensors suitable for point-of-need detection of mycotoxins.

Keywords: Optical biosensors; mycotoxins; direct immuno- or aptamer assay; TIRE; LSPR; polarization interferometry.

*corresponding author, e-mail: a.nabok@shu.ac.uk, Sheffield Hallam University, City Campus, Howard street, Sheffield, S1 1WB, UK

1. **Introduction**

Mycotoxins are products of metabolism of numerous fungi species which can grow on different agriculture products, such as grains (corn, maize, rice, etc.), nuts, spices, coffee and cocoa beans, dried fruits, etc., at elevated temperatures and high humidity [1]. Therefore, mycotoxins appeared to be quite common contaminants in the above agriculture products and associated food and animal feed [1]. Furthermore, the presence of mycotoxins in animal feed causes their wider distribution in food chain, for example in poultries, meet, and milk [2]. Mycotoxins gained great deal of attention in the last 10-15 years because of their negative impact on human and animal health; many of mycotoxins are toxic, carcinogenic, and endocrine disruptive agents. The examples of three mycotoxins which were actually the subjects of study in this work are given below:

Aflatoxins B1 and M1 (AFT B1 & M1) **[**3**]** produced by *Aspergillus flavus* and *A. parasiticus* species grown on grains and cereals (maize, rice, wheat, etc.), spices (chilli and black pepper, coriander, turmeric, ginger), tree nuts (almond, pistachio, walnut, coconut, brazil nut); Aflatoxin B1 is one of the most carcinogenic substance known. AFT M1 being a 4-hydroxylated metabolite of AFT B1 is found in caw and sheep milk and milk products.

Ochratoxin A (OTA) [4] produced by *Aspergillus ochraceus*, *A. carbonarius*, and *Penicillium verrucosum* is one of the most abundant contaminant in grain and pork products, coffee, dried grapes, also in wine and beer, [5]. OTA is carcinogenic and neurotoxic for humans, and immunotoxic for animals.

Zearalenone (ZEN) [6] produced by *Fusarium or Giberella* species grown on crops (maize, barley, oats, wheat, rice, also bread) is a potent oestrogen metabolite causing infertility in swine and poultry.

The danger of mycotoxins was well-recognised worldwide, and recent legislations set quite strict limits for mycotoxins' content in food and feed [7]. The allowed dosage is slightly varied depending on the type of agriculture products, foods, and feeds. The lowest limits for mycotoxins in single ppb (part per billion) and even below (0.05ppb for baby food) are established in EU, with similar standards in China and Japan, while US legislation is more lenient. More detailed information for particular products is available in [7]. The detection of small mycotoxin molecules (with molecular weight in 300-400 g/mol) in such small concentrations is a formidable task though not impossible. Modern analytical methods of mass-spectroscopy and chromatography are well-capable of detecting mycotoxins in ppt level of concentrations. However such advanced analytical methods are usually expensive and available in specialised laboratories; their use requires highly trained technical and academic personnel which makes the analysis very expensive and time consuming.

Much preferable solution would be portable and easy-to-use biosensor devices suitable for express, in-field detection of mycotoxins. The development of biosensors for mycotoxins has risen sharply in the last decade with a large number of different biosensing technologies been used which were extensively reviewed in [8-13]. According to review in optical biosensing of mycotoxins [10], the traditional SPR method allowed the detection of OTA down to 1.5ng/ml in concentrations, while the use of LSPR in functionalized gold nanoparticles reduced LOD substantially down to 0.04ng/ml. The SPR LODs for AFT B1 and ZON are, respectively, of 0.2 ng/ml and 0.3 ng/ml. Electrochemical detection of mycotoxins reviewed in [11] appeared to be more sensitive, for example LOD of 0.5 ng/ml for OTA detection with impedance spectroscopy; the use of aptamers in electrochemical detection of mycotoxins allowed decreasing LOD to 0.03 - 0.8 ng/ml for OTA, and 0.01 ng/ml for AFT B1.

Our contribution to development optical biosensors for mycotoxins was in the use of total internal reflection ellipsometry (TIRE) [14-17]. More detailed description of TIRE will be given in the following sections below. Briefly, this method is based on a combination of highly sensitive spectroscopic ellipsometry instrumentation with convenient Kretchmann SPR geometry. The TIRE

method, which is based on optical phase detection, appeared to be much more sensitive than conventional SPR and thus extremely suitable for detection of low molecular weight analytes such as mycotoxins [15].

In this work, we developed the TIRE method further by combining it with the effect of LSPR (localized surface plasmon resonance). Detailed study of optical properties of gold nano-structures exhibiting LSPR phenomenon is given in this work followed by a series of bio-sensing tests of detection of several previously mentioned mycotoxins, e.g. aflatoxin, ochartoxin, and zearalenone. Another optical phase-sensing method of polarisation interferometry based on planar optical waveguides is proposed here in a view of development of highly sensitive and portable (hand-held) optical biosensor devices suitable for in-field detection of mycotoxins.

2. Bio-receptors for detection of mycotoxins

Before going into details of optical techniques of TIRE, LSPR, and PI, which act as optical transducers converting bio-chemical processes into measurable optical parameters, it will be useful to discuss the bio-chemical aspects of detection of mycotoxins. The actual "detection" and "recognition" of our analytes of interest, e.g. mycotoxins, is achieved with the use of bio-receptors which are capable of their selective binding. The most common bio-receptors are antibodies which can be produced against particular targets, in our case mycotoxins. Bio-sensors based on the use of antibodies, usually called immunosensors, are the most common in optical biosensing. Antibodies are typically immobilized on the surface of optical transducers (metal films, optics fibers, nano-particles, etc.) using well-developed immobilization routes including covalent binding, electrostatic binding, encapsulation into polymer matrix, etc. Although, the strongest and thus the most stable covalent biding is commonly used in majority of optical immunosensors, in our work we used more simple method of electrostatic immobilization of antibodies which is the second strongest after covalent binding. A shown in Figure 1, IgG type of antibodies being negatively charged at pH 7-8 can be electrostatically bound to a positively charged layer of polycations, such as poly-allylamine hydrochloride (PAH) or poly-ethylenimine (PEI) previously adsorbed on the transducer surface [18]; in this case IgG molecules are randomly oriented (Fig. 1a). Much better results (tripled sensitivity) can be obtained with the use of an intermediate body, i.e. proteins G or A (depending on the type of IgG used), which are electrostatically immobilized first on PAH (or PEI) layer followed by adsorption of IgG molecules having a binding site at the second domain to protein A (or G) [15]. In this case, IgG molecules are mostly oriented "vertically" with their Fab-fragments available for biding analyte molecules as shown in Fig. 1b.

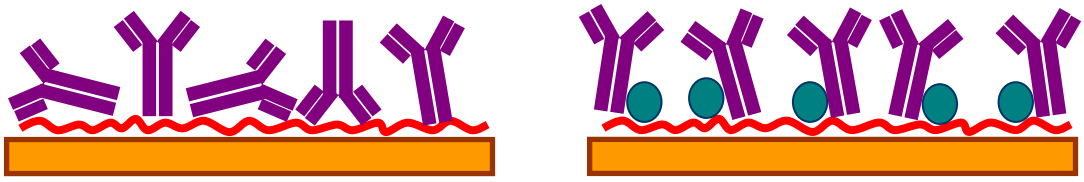

(a) (b)

Figure 1. (a) Randomly oriented antibodies immobilized directly on polycation layer; (b) vertically oriented antibodies immobilized via intermediate layer of protein G (or A).

The electrostatic immobilization of proteins including antibodies proved to be successful in our previous research [14-17], and we also used it in the current work. The immobilization procedure described previously in [14-18] was simple and consisted of consecutive immersions (injections) of PAH (1mg/ml aqueous solution for 15-20 min, protein A (or G) (0.01mg/ml solution in 35mM Tris-HCl buffer, pH 7.5 for 15 min, and IgG-based antibodies (typically 1μg/ml solution in Tris-HCl buffer pH 7.5 for 15 min.) with intermediate 3-times rinsing with de-ionized water (after PAH) and Tris/HCl buffer.

As shown schematically in Figure 2, a simple splitting IgG-based antibodies by cutting di-sulphide bonds between two heavy chains through treatment with 2-mercaptoethylamine (stage 1) has resulted in two half-antibodies with thiol groups available for subsequent covalent binding on the surface of gold (stage 2) [19]. According to this study, the other di-sulphide bonds as well as fab-fragments in IgG are not affected. The half-antibodies for aflatoxin B1 were used in the current work; the immobilization protocol was similar to that described in [19].

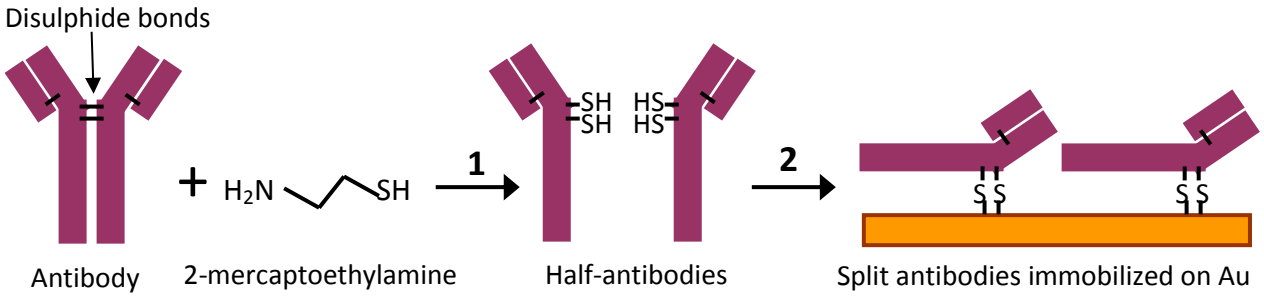

Figure 2. Splitting antibodies in 2-mercaptoethylamine (1) and their subsequent immobilization on gold via native SH groups (2).

Another possibility resulting in even smaller bio-receptors lies in the use of so-called nano-bodies which are just the variable fragments VL or VH of IgG-based antibodies [20] or variable fragments of camelid antibodies [21].

Another type of bio-receptors commonly used these days instead of antibodies are aptamers. Aptamers are synthetic oligonucleotide or peptide molecules that reproduce a similar to antibodies function, i.e. specific binding of particular target molecules. Aptamers are typically based on RNA or DNA oligonucleotides of particular sequence complementary to that of target molecules [22]; they are assembled from a vast pool of amino acids using the SELEX (systematic evolution of ligands by exponential enrichment) procedure. Aptamers have a number of advantages over traditional antibodies which include better stability, much simpler and more ethical (without the use of immunization of small animals) synthesis, and, not least, the lower price. The popularity of using aptamers as bio-receptors has rocketed in the last decade, and nowadays aptamers were commercially produced by specification for a wide range of targets. The presence of a thiol group at one end allowed simple immobilization of aptamers on gold, the other end could be either label-free or may contain functional groups, i.e. redox groups or luminophores (see Figure 3). The aptamers change their conformation (in simple terms, wrapped around the target molecules) upon binding.

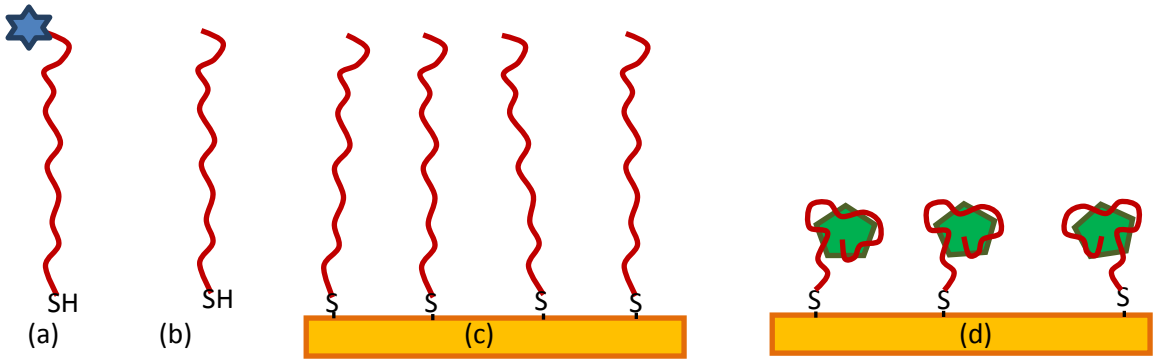

Figure 3. Schematic representation of aptamers: labelled (a), non-labelled (b), immobilized on the surface of gold (c), and rapped around target molecules (d).

Aptamers labelled with redox groups were successfully used for electrochemical detection of OTA [23]. Recently, we used similar anti-OTA aptamers, though without label, in combination with the TIRE method, and achieved the detection of OTA down to 0.01 ng/ml concentrations [24].
In the current work, we used non-labeled aptamers (from Microsynth, Switzerland) for AFT B1 having the following nucleotide sequence:

SH-5'-GTTGGGCACGTGTTGTCTCTCTGTGTCTC-GTGCCCTTCGCTAGGCCCACA-3'
with SH group at 5' (or C5) terminal and label-free terminal 3' (or C3).
The immobilization of aptamers on gold surface was carried out following the procedure described in detail in [23, 24]: the original 100 μM aptamer solution was mixed with 2 mM of 1,4-Dithiothreitol diluted in 100 mM HEPES buffer (pH 7.4) containing 2mM of $MgCl_2$, the latter was used to protect aptamers from self-coiling [23, 24]. Before immobilization, the liquid aptamer samples were activated by quick (5 min) heating up to 90°C followed by 5 min cooling to 4°C using thermo-cycling PCR unit. Immobilization was carried out by casting aptamer solution onto gold coated slides; the immobilization time was 4 hours at room temperature in moist atmosphere. The unreacted oligonucleotide was removed from the gold slides by several rinsing stages with HEPES/$MgCl_2$ buffer. The immobilized aptamers are prone to self-coiling. In order to prevent that and keep aptamers active, the gold coated glass slides with immobilized aptamers were kept in HEPES/$MgCl_2$ buffer. The samples with immobilized aptamers were quite stable and keep their functionality for few weeks. Interestingly, the old samples with immobilized aptamers could be reactivated by thermo-cycling in PCR machine.

3. Total Internal Reflection Ellipsometry (TIRE)

The method of TIRE, which was proposed by Arvin [25] and later developed further in our research group [14-17], combines the advantages of high precision spectroscopic ellipsometry instrumentation and experimental convenience of Kretchmann SPR. Our experimental set-up, shown schematically in Figure 4a, is based on J.A. Woollam M2000 spectroscopic ellipsometer with the addition of 68° prism through which the light is coupled to thin (25nm) of gold deposited on a microscopic glass slide.

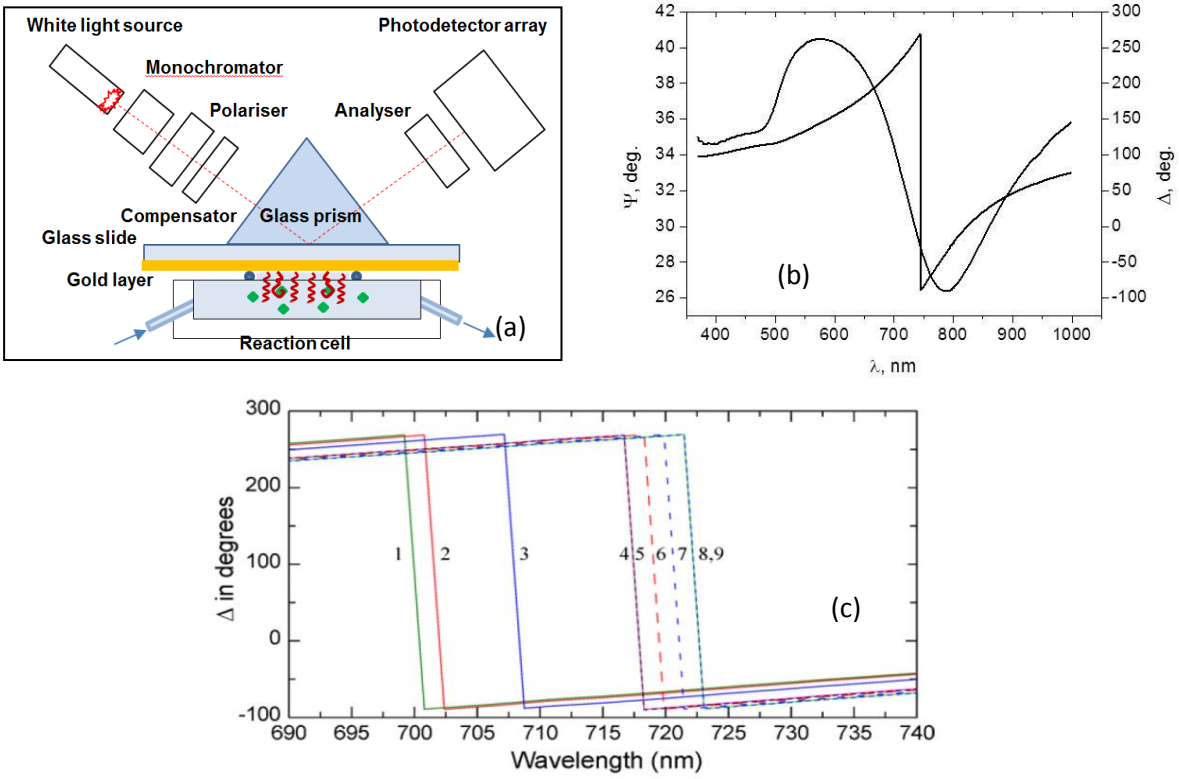

Figure 4. (a) Schematic diagram of TIRE experimental set-up; (b) typical TIRE spectra of Ψ and Δ for 25nm thick Au film deposited on glass [16]; and series of Δ spectra recorded on bare Au (1) and after adsorption of PAH (2), protein A (3), antibodies to ZON (4), and consecutive binding of ZON in concentrations increasing from 0.1ng/ml to 1μg/ml (5-9) [16].

The main advantage of TIRE is the use of two ellipsometric parameters Ψ and Δ, which are related, respectively, to the ratio of amplitudes and phase shift of p- and s- components of polarized light ($tan\,\Psi = A_p/A_s$, $\Delta = \varphi_p - \varphi_s$) as compared to SPR operating with the amplitude of p- polarized light. As one can see from Figure 4b, the spectrum of Ψ resembles typical SPR curve with the minimum at about 800 nm corresponding to plasmon resonance, while the spectrum of Δ exhibits a sharp drop of phase near the resonance. The ellipsometry data modeling showed that the parameter Δ is about 10 times more sensitive to changes in the film thickness and refractive index as compared to Ψ [15]. In other words, the method of TIRE appeared to be 10 times more sensitive than conventional SPR.

As shown in Figure 4c, deposition of molecular layers of PAH, protein A, and antibodies causes a progressive "red" shift of Δ-spectra associated with the increase in the molecular layer thickness which in turn correlated to the size (or mass) of molecules. Similarly, binding of mycotoxin molecules to specific antibodies causes a noticeable “red” spectral shift which could be calibrated against the concentration of analyte molecules, and thus served as a sensor response. It has to be noted that TIRE spectroscopic scans were carried out in the same Tris/HCl (pH 7.5) buffer solution after purging 1ml (5 times of a cell volume) of buffer through the cell; this was to remove non-specifically bound toxin molecules.

Alternatively, the ellipsometry data fitting can be carried out in order to evaluate the thickness of the adsorbed molecular layer as a physical measure of molecular adsorption. Such data fitting was performed with J.A.Woollam software using a four-layer model, which was described in details earlier [15]. In our research we usually perform TIRE data fitting which provides high accuracy of thickness measurements down 0.01nm.

Our previous research in detection of several different mycotoxins (T2, aflatoxin B1, and zearalenone) was successful, and allowed the detection of the above mycotoxins in low concentrations down to 0.1ng/ml (or 0.1ppb) in direct immunoassay with specific (whole) antibodies electrostatically immobilized on gold surface [14-17], while competitive immunoassay yielded lower LDL of 0.01ng/ml [16]. The time of analysis, excluding immobilization of antibodies takes about 10-15 min. It has to be noted that competitive immunoassay, despite of its higher sensitivity, is more expensive (since required large amount of antibodies) and takes longer time. The method of TIRE appeared to be particularly useful for detection of low molecular weight analytes such as mycotoxins, and the achieved LDL in 0.1 ppb fits well to high demands of EU legislation. These results were particularly impressive because of the use of a simple and inexpensive direct immunoassay format.

4. Localized surface plasmon resonance (LSPR) and its application in biosensing.

The phenomenon of localized surface plasmon resonance (LSPR) is related to interaction of external electromagnetic waves with localized surface plasmons, e.g. oscillations of free electrons, confined into small volumes comparable with the wavelength of light. LSPR is typically observed in metal nano-structures, for example nanoparticles, as an absorption band in a visible spectral range. The phenomenon of LSPR has been described theoretically by Mie more than a century ago (well before the quantum mechanics was established) as a light scattering on conductive (metal) spherical particles of dimensions comparable with the wavelength of light. This effect known as Mie scattering [26] is described by the following dispersion characteristic of light absorption:

$$\sigma_{ext} = \frac{9V\varepsilon_m^{3/2}}{c} \frac{\omega\varepsilon''(\omega)}{\left[\varepsilon'(\omega) + 2\varepsilon_m\right]^2 + \varepsilon''(\omega)^2},$$

where σ_{ext} is the extinction cross-section, $\varepsilon'(\omega)$ and $\varepsilon''(\omega)$ are dispersions of the real and imaginary parts of dielectric permittivity of metal, respectively, ε_m is the dielectric permittivity of the

medium, and V is the particle volume. The extinction maximum (resonance) is achieved when $\varepsilon'(\omega) = 2\varepsilon_m$ (ε' is negative for metals). Therefore, the position of LSPR band depends on the medium refractive index. The latter fact actually constitutes the main principle of LSPR biosensing; small changes in the refractive index due to molecular adsorption cause the "red" spectral shift of the LSPR band.

The interest to LSPR has grown dramatically recently due to its possible applications in biosensing, and was also stimulated by fast evolvement of nanotechnology which is now capable of producing different types of metal nanostructures. For a while, LSPR was only observed in metal nano-particles [27, 28], then many other types of LSPR nanostructures such as nano-rods [29, 30], nano-islands [31, 32], nano-holes [33, 34], appeared in recent years. Such nanostructures could be mono- or poly-dispersed in terms of their dimensions; their spatial distribution could be either random or ordered. The 2D ordered metal nano-structures can be produced using different types of nano-lithography, i.e. electron beam lithography [35], interference lithography [36], and nano-sphere lithography [37]. Noble metals such as gold and silver are commonly used for the formation of nano-structures; aluminum and copper were also used. Although Ag nano-structures have the best LSPR characteristics, e.g. the sharp plasmon resonance [28], gold nano-structures are the most popular due to the chemical stability of gold and well-developed thiol-chemistry of immobilization of proteins on gold surface [34, 36]. The theory of LSPR has been developed further using the concept of quantum confinement of surface plasmons in different metal nano-structures of different dimensions and shapes, and now appeared as a new the subject of quantum plasmonics [38-40]. The appearance of multiple LSPR peaks can be explained by quantization of plasmons in different directions [40].

The applications of LSPR in bio-sensing have become very attractive recently mainly because of potentially extremely high sensitivity of LSPR bio-sensors [34, 40-42]. The term "single molecule detection" has become associated with LSPR bio-sensors. Another attraction is deceivingly simple instrumentation for LSPR biosensing; a simple UV-vis spectrometer with the cuvette filled with gold nanoparticles functionalized with specific antibodies can be capable of detection of the analytes of interest. In reality, the sensitivity of such LSPR biosensors is rather poor. Although, the adsorption of a single protein molecule on a metal nanoparticle may indeed cause a substantial shift of the LSPR band, in reality the light beam of few square millimeters probes millions of such particles, and the resulted spectral shift may be unnoticeable. As a result such simple LSPR bio-sensors are capable of detection of large protein molecules in ppm concentration range [43]; and the detection of small molecules is only possible in competitive or sandwich immunoassay formats [43]. True single molecule detection was achieved only recently using extremely fast camera capable of capturing the light scattered by individual metal nano-rods passing through microfluidic channels [44]; these experiments are quite unique and require expensive optical equipment.

5. Fabrication and characterization of gold nano-islands, LSPR/TIRE combination.

One of the easiest methods of making gold nano-structures is annealing of thin gold films which results in the formation of gold nano-islands due to de-wetting processes [45]. Typical annealing temperatures are around 500 ^{O}C and duration for 1 to 2 hours. In order to improve the adhesion of gold on glass a thin (2-3nm) layer of Cr has to be evaporated first [46]. Alternatively, the annealing at slightly high temperatures (550 ^{O}C) and longer time (up to 10 hours) can be used, resulting in stable gold nano-islands embedded into a glass matrix [32]. The latter method was eventually selected in our work after exploring different regimes of gold evaporation and annealing.

A series of samples were prepared by evaporating gold of different thicknesses of 4, 5, 6, and 10 nm on microscopic glass slides preliminary cleaned in piranha solution. The evaporation was carried

out in Edwards 360 unit at the vacuum of 10^{-6} Tor. The nano-islands were formed by annealing at $550C^{O}$ for 10 hours.

The samples produced were characterized with SEM (FEI-Nova, NanoSEM 200), AFM (Nanoscope IIIa, Bruker), UV-vis absorption spectroscopy (Cary 50, Varian), and spectroscopic ellpsometry (J.A. Woollam, M2000). Typical SEM and AFM images of nano-islands produced by annealing of 5nm thick gold film are shown in Figure 5 [46]. The analysis of SEM images for all samples studied given in Table 1 showed gradual increase in both the average diameter and average thickness of gold nano-islands with the increase in the nominal thickness of Au films.

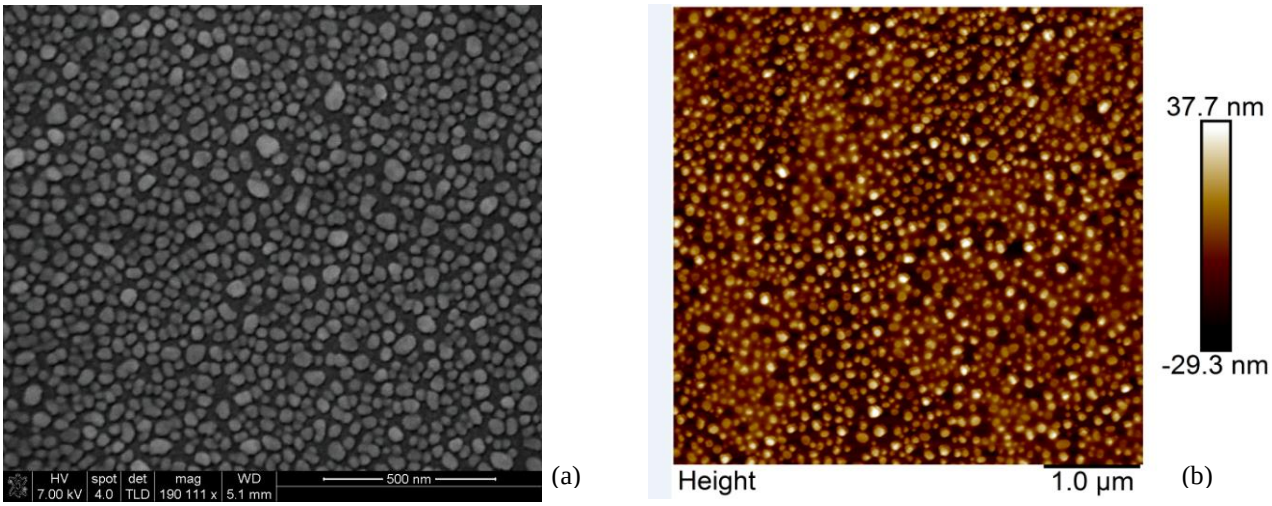

Figure 5. Typical SEM (a) and AFM (b) images of Au nano-islands [46].

Table 1. The results of AFM image analysis of gold nano-structures.

Nominal Au film thickness	4 nm	5 nm	6 nm	8 nm	10 nm
Island height (nm)	5.7 ± 1.0	12.2 ± 2.3	9.6 ± 2.5	13.9 ± 2.4	34.1 ± 6.6
Island diameter (nm)	29.9 ± 6.6	35.0 ± 12.0	71.7 ± 12.6	68.2 ± 10.7	90.9 ± 25.0

The UV-vis absorption spectra of annealed thin Au films showed a pronounced LSPR peak in the middle of visible spectral range position of which is gradually shifted to high wavelengths upon increasing in the nominal film thickness [46]. More detailed study of optical properties of nano-structured Au films was carried out using spectroscopic ellipsometry. Typical ellipsometry spectra of gold nano-structures produced are shown in Figure 6. Ψ spectra resemble SPR curves with the minima corresponding to plasmon resonance, while Δ spectra have a characteristic drop of phase near plasmon resonance.

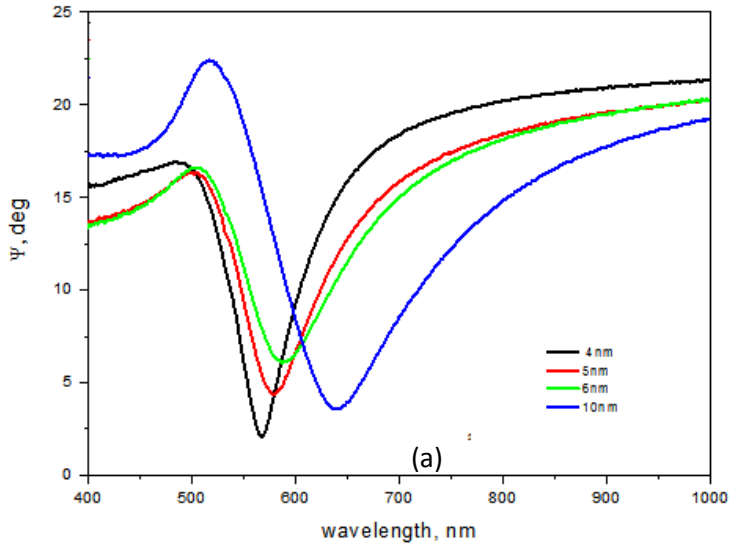

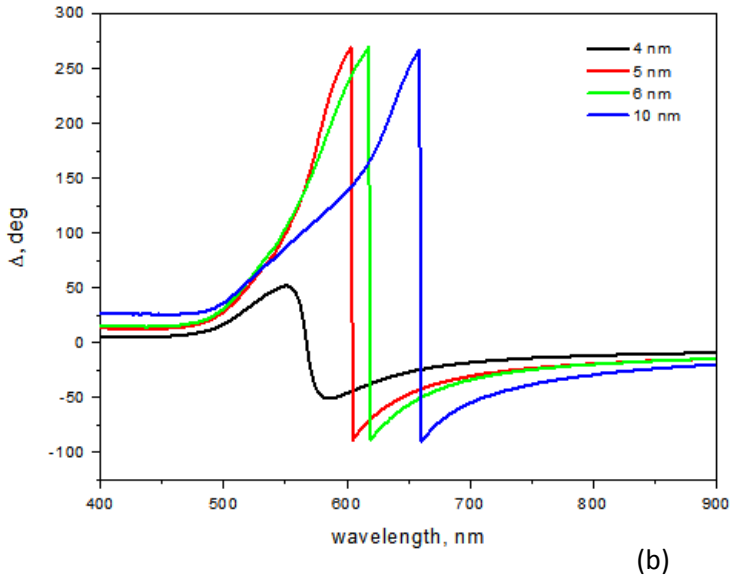

Figure 6. Spectroscopic ellipsometry spectra of a series of gold nano-structures made from different nominal films thicknesses: (a) Ψ spectra; (b) Δ spectra.

Ellipsometry data fitting was carried out using J.A. Woollam CompleteEase software. The nanostructured gold film was modelled by a combination of Drude dispersion function and three additional Gaussian oscillators; two of them (E_x and E_y) have similar energies around 2 eV and most likely correspond to quantization of plasmons in lateral directions (x, y) of Au nano-islands, while the third one (E_z) around 5 eV may corresponds to plasmons' quantization in vertical direction (z), e.g. the thickness of Au nano-islands. The resulted values of the average gold film thickness as well as the Gaussian oscillator energies are given in Table 2.

Table 2. The results of ellipsometry data fitting.

Nominal thickness (nm)	4	5	6	10
Measured thickness (nm)	3.48	5.18	6.87	16.34
E_x (eV)	2.197	2.179	2.175	2.121
E_y (eV)	2.145	2.032	2.034	1.960
E_z (eV)	5.174	4.309	6.039	1.778

As one can see, the obtained values of gold film thickness, which is an average of the thickness of nano-islands and the empty space between them, correlate reasonably with the nominal thickness of Au films. The dispersion characteristics of refractive index (n) and extiction coefficient (k) obtained by ellipsometry data fitting are given in Figure 7.

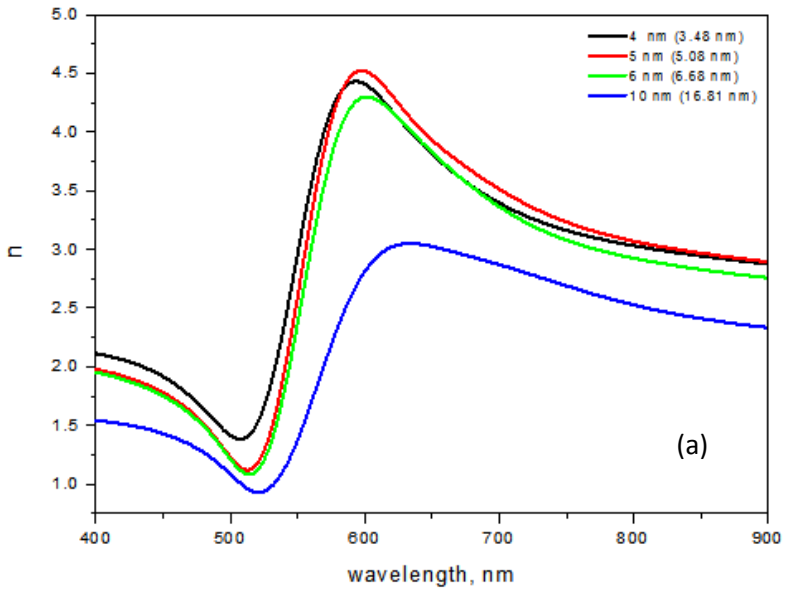

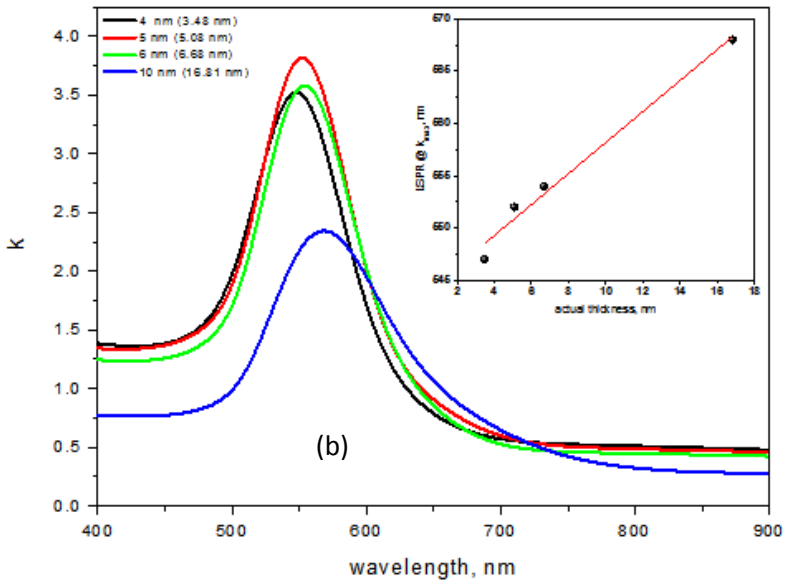

Figure 7. Dispersion characteristics of *n* (a) and *k* (b) obtained by ellipsometry data fitting. Inset shows the dependence of the position of LSPR peak on the actual gold film thickness.

The resulted spectra of *n* and *k* are Kramers-Kronig consistent, e.g. peaks on *k*- spectra, which correspond to LSPR, coincide with the largest gradient on *n*- spectra. The inset in Fig. 7a shows linear increase in the LSPR position against the actual gold film thickness. The LSPR peak positions are very close to those found with UV-vis absorption spectroscopy [46].

Both UV-vis absorption spectroscopy and spectroscopic ellipsometry show features associated with LSPR. The refractive index sensitivities (RIS) of these two experimental methods were compared by carrying out measurements in media of different refractive indices [46]. The results surprisingly showed higher RIS values for ellisometry measurements. The RIS_{SE}/RIS_{Abs} ratio increases from 2.15 for larger Au nano-islands (nominal thickness of 10nm) up to of 3.27 for small Au nano-islands (nominal thickness of 4nm) [46]. These experimental facts can be understood considering multiple reflections of light in ellipsometry (three reflections are essential) as compared to a single interaction in absorption spectroscopy. Therefore the reflected electromagnetic wave can probe several nano-islands, which explains the dependence on the island size.

Another interesting property of metal nano-structures is much shorter evanescent field decay length as compared to that in total internal reflection geometry [43]. The experimental study of that effect was carried out by monitoring the LSPR spectral shift during deposition of polyelectrolyte layers, i.e. PAH and PSS [47]. The saturation of the spectral shift observed experimentally fits into rising exponential function, thus allowing the evaluation of the decaying length. It appeared that the evanescent field decay length varies from 16 nm for small Au-nano-islands (4nm nominal thickness) up to 31nm for large Au nano-islands (10nm nominal thickness) [47]. Such values are much smaller that evanescent decay length of 100-200 nm in traditional SPR experiments. This fact has serious implications on LSPR biosensing, particularly on the dimensions of bio-receptors used.

6. Detection of mycotoxins using a combination of LSPR/TIRE.

The superior RIS of ellipsometry inspired us to use TIRE geometry for LSPR bio-sensing. However, our initial attempts of using LSPR/TIRE combination for detection of aflatoxin B1 in direct immunoassay with specific whole) antibodies electrostatically immobilized on the surface of gold nano-islands were not successful [48]. The spectral shift of Δ was observed only at concentrations of AFT B1 of 1ng/ml (1 ppb) and saturated quickly at about 100ng/ml (100ppb) [48]. The sensitivity was 2 orders of magnitude lower than that in our traditional TIRE biosensing

using continuous 25nm thick Au layers [17]. The explanation of that was in the use of large size bio-receptors, e.g. whole IgG-based antibodies electrostatically immobilized via layers of protein A and PAH, with the thickness of bio-receptor layer being comparable or even larger than the evanescent field decay length of 20 nm for Au nano-structures with the nominal thickness of 5nm used in these measurements.

As was expected, the use of small size bio-receptors, such as half-antibodies immobilized on the surface of gold via native thiol groups (see Figure 2), yields much better results in LSPR/TIRE method [49]. The TIRE measurements on detection of AFT B1 in direct immunoassay with respective half-antibodies immobilized on the surface of gold nano-islands revealed progressive "red" shift of Δ spectra (see Figure 8a). Figure 8b showed a monotonous increase of the spectral shift with the increase in concentration of AFT B1 with a trend of saturation at high concentrations of 1μg/ml. A substantial spectral shift of about 2.5 nm was recorded upon binding of 0.01 ng/ml (the lowest concentration used in this work) of AFT B1 [49]. The non-specific binding of AFT B1 was eliminated by rinsing the cell with buffer after each binding step, as was described earlier. Considering the accuracy of TIRE spectral measurements of about 0.1nm it can be concluded that much lower (at list by one order of magnitude) concentration of AFT B1 can be detected with the combination of TIRE and LSPR.

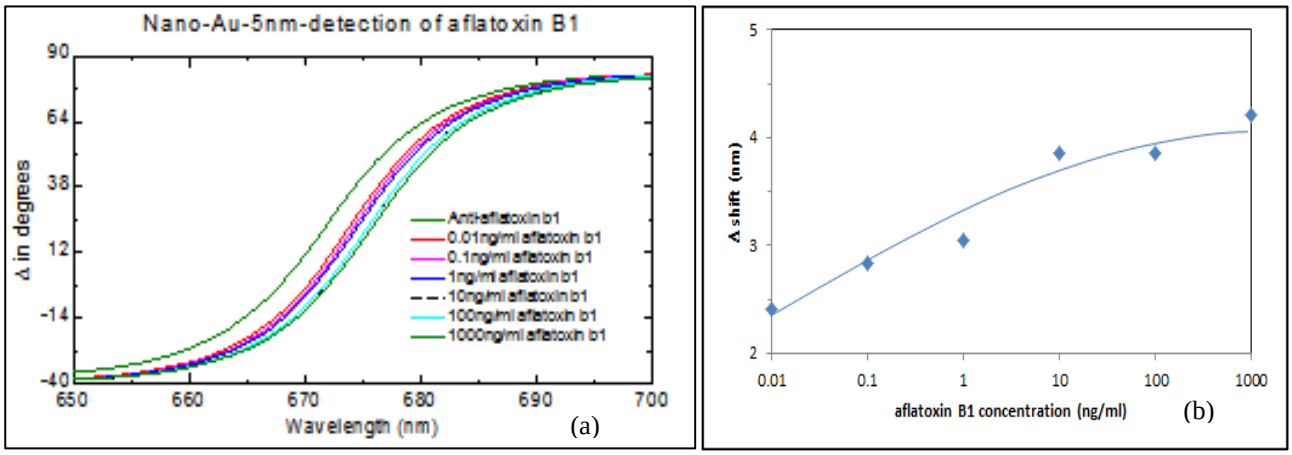

Figure 9. (a) Series of TIRE Δ spectra recorded on 5nm Au nanostructures upon binging AFT B1 of different concentrations to split antibodies, (b) calibration curve for AFT B1 [49].

The study of the aflatoxin/aptamer binding kinetics which was carried out by performing dynamic spectral measurements and subsequent data analysis described in detail previously in [14-17, 49, 50] allowed the evaluation of the association (K_A) and affinity (K_D) constants. The values for half-antibodies specific to AFT B1 were found as $K_A = 4.6 \times 10^7$ (mol^{-1}) and $K_D = 2.1 \times 10^{-8}$ (mol), which are very similar to respective values for whole antibodies [17]. This proved once again, that Fab-fragments of antibodies are not affected by splitting di-sulphide bonds in the constant domain.

Similarly successful results were obtained on LSPR/TIRE detection of AFT B1 in aptamer assay [50]. Aptamers specific to AFT B1 were immobilized on Au nano-islands of nominal thickness of 5nm as described earlier in section 2. As shown in Figure 10a, binding of AFT B1 molecules to aptamers caused the "blue" shift of Δ spectra (the opposite to the "red shift" for antibodies), which corresponds to the reduction in the molecular layer thickness. Indeed, the calibration curve on Fig. 10b obtained by TIRE data fitting shows the reduction in the aptamer layer thickness from its initial value of 2.09nm down to 1.8nm upon binding of AFT B1 caused by aptamers wrapping around their target (see illustration in Fig. 3). Considering the accuracy of ellipsometry thickness measurements of 0.01nm, the 0.03nm reduction in the aptamer layer thickness (from 2.09 nm to

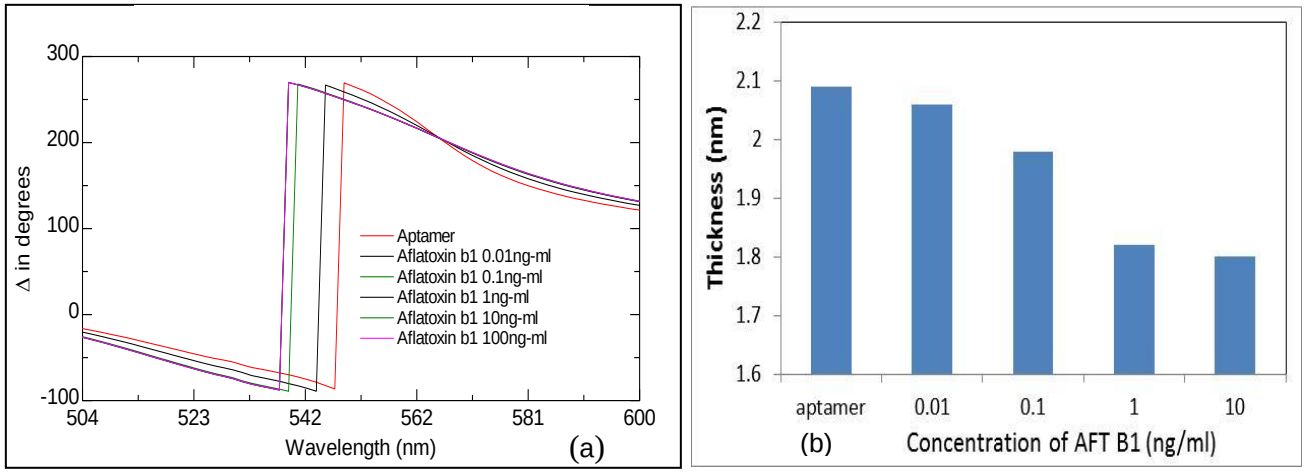

Figure 10. (a) Series of TIRE Δ spectra recorded on 5nm Au nanostructures upon binging AFT B1 of different concentrations to aptamers, (b) calibration curve for AFT B1 in aptamer assay [50].

2.06nm) as a result of binding of 0.01ng/ml of AFT B1, 3 times high than the thickness resolution can define the LDL as 0.01ng/ml. The saturation of the response was observed at much smaller concentrations of AFT B1 of about 10ng/ml. This situation could be improved and the dynamic range of detection extended if we use higher concentration of aptamers.

The binding kinetics yielded the values of $K_A = 3.12 \cdot 10^7$ (mol^{-1}) and $K_D = 3.2 \cdot 10^{-8}$ (mol) for anti-AFT B1 aptamers [49] which is very similar to corresponding values of whole [16] and halved [49] monoclonal antibodies to AFT B1. It proves once again the high specificity of aptamers towards binding their specific targets.

The use of aptamers as small size bio-receptors for mycotoxins suits perfectly to LSPR/TIRE method. The other advantages of aptamers are their high stability and relative simplicity of immobilization. The immobilization of aptamers can be done in advance, and the samples with immobilized aptamers can be kept in binding buffer (containing $MgCl_2$ salt) in the fridge for weeks. In case of losing functionality, the immobilized aptamers can be reactivated by thermo-cycling in PCR unit as described in section 2.

7. Miniaturisation of optical biosensors: planar waveguide biosensors

The problem of optical detection of small toxin molecules seemed to be resolved; the method of TIRE which is based on optical phase detection is capable of detection of mycotoxins down to 10 ppt concentrations and perhaps even below. The use of small size bio-receptors is beneficial, particularly for LSPR. However, the spectroscopic ellipsometry is still lab-based equipment, bulky, expensive, and not easy to use. What shell we do to fulfill the current demands of portable biosensors suitable for point-of need analysis? The answer lies in the use optical sensors based on phase detection, i.e. interferometers. Several recent developments of such devices proved to be successful [51]; they include dual polarization interferometers [52-54], ring-resonators [55], and Mach-Zehnder (MZ) interferometers [52, 56-58]. Biosensors based on MZ interferometers are perhaps the most popular devices which combine high sensitivity of detection and portable design [52, 56-58]. The development of a monolithic silicon-based MZ biosensor [59, 60] combining the light source, photo-detector, and multichannel waveguide equipped with microfluidic is particularly promising for point-of-need sensor development.

The biosensor explored in this work is based on a planar waveguide similar to that used in MZ devices but with much simpler design. The proposed sensor design is shown schematically in Figure 11. Instead of two arms in MZ interferometer, we use a single waveguide channel made of Si_3N_4 200 nm thick layer sandwiched between two much thicker (1-3 mm) SiO_2 layers with a sensing window etched in the top SiO_2 layer. The biosensing molecular layer can be deposited in

the sensing window. A circularly polarized light is coupled through the slant edge of the waveguide and propagates at a steep angle of 47^o due to a large difference in refractive indices between Si_3N_4 core (n=2) and SiO_2 cladding (n=1.46). Upon the propagation of polarized light, its p-component is mostly affected by changes in the refractive index (or thickness) in the biosensing layer, while s-component is practically not affected and serves a reference. As a result, a phase shift between p- and s- components of polarized light is developed and can be detected using a polarizer on the output. The resulted output waveform is multi-periodic and could be converted to the time dependence of a phase shift, which constitute the actual sensor response.

The device described above is a polarization interferometer which has been proposed quite long time ago [61, 62] but was not fully explored that time. Similar type of waveguide, though operating as an optrode, was successfully used in the sensor array for detection of traces of heavy metals and pesticides in ppb concentrations [63]. The main advantage of the PI biosensor is its potentially extremely high sensitivity due to a large number of reflections (about 1000 per mm) in the waveguide, and the expected sensitivity is in ppt range of concentration [62].

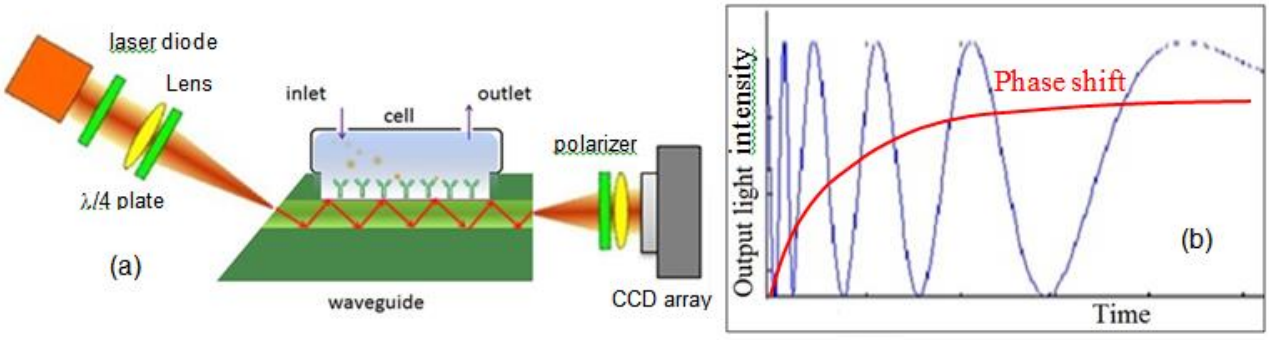

Figure 11. (a) Design of polarization interferometer based on planar waveguide; (a) output waveform and corresponding phase shift.

The experimental set-up for PI biosensor equipped with the reaction cell and inlet and outlet tubes for injection of solutions to be analysed was built and tested [64]. The refractive index sensitivity was evaluated by injecting liquids of different refractive indices (different concentrations of NaCl) and appeared to be of 5300 rad/RIU which is close to that reported for MZ-based biosensors [51].

Series of biosensing tests on detection of ochratoxin A (OTA) were carried out in direct immuno-assay with specific whole antibodies immobilized electrostatically in the sensing window [65] (the immobilization protocol was described in section 2), and the results are shown in Figure 12.

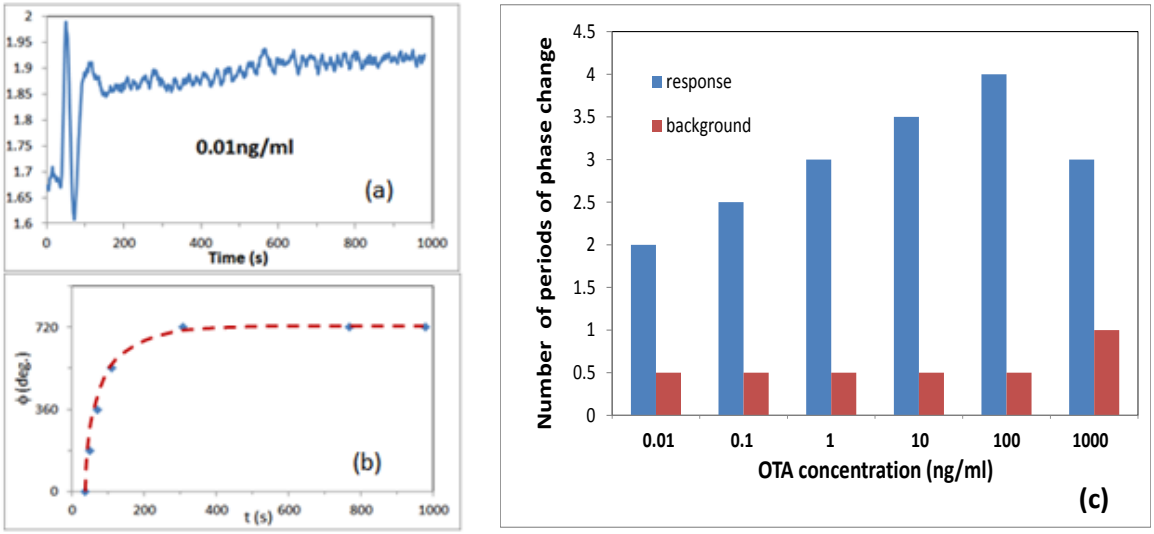

Figure 12. (a) Output signal recorded during binding 0.01ng/ml of OTA to specific antibodies; (b) corresponding phase shift; (c) concentration dependence of PI sensor response [65].

As an example, a typical multi-periodic output waveform for the smallest concentration (0.01ng/ml) of OTA used and its conversion to the responding phase shifts are shown in Figures 12a and 12b, respectively. Such measurements were carried out by sequential injections of OTA in progressively increased concentrations with intermediate washings out of non-specifically bound toxins by purging buffer solution through the cell. The results for all OTA concentrations studied were summarized in Fig. 12c as a phase shift vs. OTA concentration. The accuracy of phase shift evaluation is about ¼ of a period. As one can see, the response (blue pols) increases monotonously with the concentration until 100ng/ml, then the phase shift went slightly down at 1000ng/ml most-likely because of the saturation of binding cites, e.g. antibodies. The process of washing out no-specifically bound OTA is usually resulted in a half-a-period phase shift shown as red pols in Fig. 11c; it went up to a whole period at the largest OTA concentration which is another indication of the saturation of binding cites. The negative control tests were carried out, for example by exposing anti-OTA antibodies to AFT B1toxin; such tests showed no response.

Similar measurements were carried out on the other mycotoxins, i.e. aflatoxin B1 B1 [64] and zearalenone. The results were summarized in Figure 13 as accumulated response (phase shifts of previous exposures were added up and washing out responses subtracted) against the total mycotoxin concentration, e.g. 0.01, 0.11, 1.11, 11.11, 111.11, and 1111.11 (ng/ml).

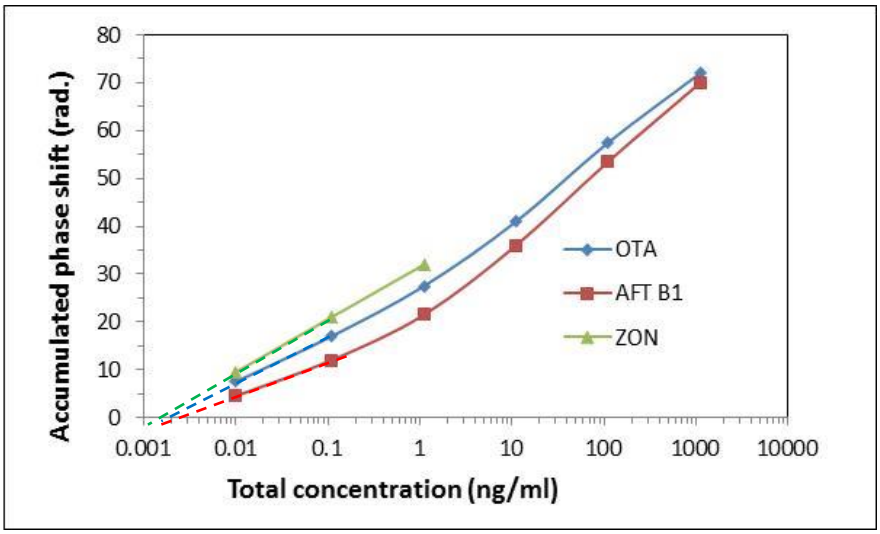

Figure 13. Accumulated response of PI sensor for three mycotoxins studied.

All three mycotoxins studied showed similar responses which are expected because of their similar molecular weight. The phase shift monotonously increases with the increase in mycotoxin concentration; a trend of saturation is showing at high concentrations of AFT B1 and OTA. The concentration range for ZON was much smaller. The accuracy of a phase shift evaluation is about 1.57 rad. The lowest concentrations of mycotoxins used was 0.01 ng/ml, however much smaller concentrations can be detected; the LOD value of about 0.002 ng/ml (or 2 pg/ml) could be estimated by linear extrapolation of the graph.

This work is still in progress, and the recent tests which were done using upgraded PI set-up having much higher RIS in the range of 9200 rad/RIU showed the detection of 1pg/ml (1 ppt) of AFT B1 in direct assay with specific aptamer [66].

8. Conclusions

The two optical methods, e.g. total internal reflection ellipsometry combined with LSPR transducers based on nano-structured gold films and planar waveguides operating as polarization interferometer, were explored here for detection of mycotoxins in direct assay with either whole

antibodies, or half-antibodies, or aptamers. A combination of TIRE with LSPR was a success; it allows the detection of low molecular weight analytes, such as mycotoxins, in concentrations down to 0.01 ng/ml (10 ppt) using a simple direct immunoassay format. The limitations of LSPR due to a short evanescent field decay length can be overcome using small bio-receptors, such as half-antibodies and aptamers.

Polarization Interferometer biosensor based on planar waveguides is one of the most promising ways forward towards development of portable and highly sensitive optical biosensors. The PI experimental set-up provides the refractive index sensitivity comparable with MZ interferometer sensors. The detection of mycotoxins in single ppt level of concentrations was achieved. The current PI experimental set-up, though still of a bench-top type, is much smaller (about 30x20x10 cm) and cheaper than the J.A. Woollam spectroscopic ellipsometer which the TIRE is based; it could be scaled down further to a hand-held type of device.

Future work is focused mostly on development of PI-based biosensors including the improvement of the sensor design, data processing, and the use of aptamers as bio-receptors. The detection of mycotoxins in real samples of food is also planned.

Acknowledgments
This work was supported by NATO SPS program, project NUKR.SFPP 984637.

References

1. Peraica, M., Radic, B., Lucic, A., and Pavlovic, M. (1999), Toxic effects of mycotoxins in humans, Bulletin of the World Health Organization, 77(9), 754-766.
2. Bhat, R., Rai, R.V., Karim, A.A. (2009), Mycotoxins in food and feed: Present status and future concerns, Comprehensive Reviews in Food Science and Food Safety, Wiley Online Library, https://doi.org/10.1111/j.1541-4337.2009.00094.x
3. Yin, Y.N., Yan, L.Y., Jiang, J.H., Ma, Z.H. (2008), Biological control of aflatoxin contamination of crops, J Zhejiang Univ. Sci. B, 9 (10), 787–92.
4. Bayman, P., Baker, J.L. (2006), Ochratoxins: a global perspective, Mycopathologia, 162 (3), 215–23.
5. Mateo, R., Medina, A., Mateo, E.M., Mateo, F., Jiménez M. (2007), An overview of ochratoxin A in beer and wine, Int. J. Food Microbiol., 119 (1–2), 79–83.
6. Desjardins, A.E., Proctor, R.H. (2007), Molecular biology of Fusarium mycotoxins, Int. J. Food Microbiol., 119 (1–2), 47–50.
7. Worldwide Mycotoxin Regulations - Romer Labs (2016), https://www.romerlabs.com/en/knowledge-center/knowledge-library/articles/news/worldwide-mycotoxin-regulations/.
8. Van der Gaag, B., Spath, S., Dietrich, H., Stigter, E., Boonzaaijer, G., Van Osenbruggen, T., Koopal, K. (2003), Biosensors and multiple mycotoxin analysis, Food Control, 14 (4), 251-254.
9. Pohanka. M., Jun, D., Kuca, K., (2007) Mycotoxin assays using biosensor technology: a review, Drug Chem. Toxicol., 30(3), 253-61.
10. Ying Li, Xia Liu, Zhao Lin (2012). Recent developments and applications of surface plasmon resonance biosensors for the detection of mycotoxins in foodstuffs, Food Chemistry, 132 (3), 1549-1554.
11. Vidal, J.C., Bonel, L., Ezquerra, A., Hernández, S., Bertolín, J.R., Cubel, C., Castillo, J.R. (2013), Electrochemical affinity biosensors for detection of mycotoxins: A review, Biosensors and Bioelectronics, 49, 146-158.
12. Evtugyn, G.A., Shamagsumova, R.V., Hianik. T. (2017), Biosensors for detection mycotoxins and pathogenic bacteria in food, Nanobiosensors, 35–92, Elsevier, Academic Press, https://doi.org/10.1016/B978-0-12-804301-1.00002-3.
13. Omrani, N.M., Hayat, A., Korri-Youssoufi, H., Marty, J.-L. (2016), Electrochemical biosensors for food security: Mycotoxins detection, Biosens. for Security & Bioterrorism Appl., Springer, 469-490.
14. Nabok, A., Tsargorodskaya, A., Hassan, A.K, Starodub, N.F. (2005), Total internal reflection ellipsometry and SPR detection of low molecular weight environmental toxins, Applied Surface Science, 246, 381-386.

15. Nabok, A., Tsargorodskaya, A. (2008), The Method of Total Internal Reflection Ellipsometry for Thin Film Characterisation and Sensing, Thin Solid Films, 516, 8993-9001.
16. Nabok, A., Tsargorodskaya, A., Mustafa, M.K., Szekacs, I., Starodub, N.F., Szekacs, A. (2011), Detection of low molecular weight toxins using an optical phase method of ellipsometry, Sensors and Actuators B: Chemical,154, 232-237.
17. Nabok, A., Mustafa, M.K., Tsargorodskaya, A., Starodub, N.F. Detection of aflatoxin B1with a label free ellipsometry immunosensor, BioNanoScience, 1 (2011) 38-45.
18. Starodub, N.F., Nabok, A., Starodub, V.M., Ray, A.K., Hassan, A.K. (2001), Immobilisation of biocomponents for immune optical sensors, Ukrainian Bio-Chemical Journal, 73 (5), 55-64.
19. Karyakin, A.A., Presnova, G.V., Rubtsova, M.Y., Egorov, A.M. (2000), Oriented immobilization of antibodies onto the gold surfaces via their native thiol groups, Anal. Chem. 72(16), 3805-3811.
20. Ahmad, M.Z., Akhter, S., Rahman, Z., Akhter, S., Anwar, M., Mallik, N., Ahmad, F.J. (2012), Nanometric gold in cancer nanotechnology: current status and future prospects, J. Pharmacy and Pharmacology, Wiley Online Library, https://doi.org/10.1111/jphp.12017.
21. Huang, L., Muyldermans, S., Saerens D. (2010), Nanobodies: proficient tools in diagnostics, Expert Review of Molecular Diagnostics, 10(6), 777-785.
22. Ellington, A.D., Szostak, J.W. (1990), In vitro selection of RNA that binds specific ligands, Nature, 346, 818-822.
23. Rhouati, A., Yang, C., Hayat, A. and Marty, J.-L. (2013), Aptamers: A promising tool for ochratoxin A detection in food analysis, Toxins, 5(11), 1988-2008.
24. Al-Rubaye, A.G., Nabok, A., Catanante, G., Marty, J-L., Takacs. E, Szekacs, A. (2018), Detection of ochratoxin A in aptamer assay using total internal reflection ellipsometry, Sensors and Actuators: B Chemical, 263, 248-251.
25. Arwin, H., Poksinski, M. and Johansen, K. (2004), Total internal reflection ellipsometry: principles and applications. Applied Optics, 43(15), 3028-3036.
26. Mie, G. (1908), Beiträge zur Optik trüber Medien, speziell kolloidaler Metallösungen, Annalen der Physik, 25 (3) 377-445, https://doi.org/10.1002/andp.19083300302.
27. Raschke, G. Kowarik, S. Franz, T., Sönnichsen C., Klar, T.A., Feldmann, J., Nicht, A., Kürzinger, K. (2003), Biomolecular Recognition Based on Single Gold Nanoparticle Light Scattering, Nano Letters, 3 (7), 935–938.
28. McFarland, A. D., Van Duyne, R. P.(2003), Single silver nanoparticles as real-time optical sensors with zeptomole sensitivity. Nano Lett. 3, 1057–1062.
29. Gabudean, A.M., Biro, D., Astilean, S. (2011), Localized surface plasmon resonance (LSPR) and surface-enhanced Raman scattering (SERS) studies of 4-aminothiophenol adsorption on gold nanorods, Journal of Molecular Structure, 993 (1–3), 420-424.
30. Zhang, Z., Chen, Z., Qu, C., Chen, L. (2014), Highly sensitive visual detection of copper ions based on the shape-dependent LSPR spectroscopy of gold nanorods, Langmuir, 30(12), 3625–3630.
31. Lahav, M., Vaskevich, A., Rubinstein, I. (2004), Biological sensing using transmission surface plasmon resonance spectroscopy, Langmuir, 20 (18), 7365–7367.
32. Karakouz, T., Tesler, A.B, Bendikov, T.A., Vaskevich, A., Rubinstein, I. (2008), Highly stable localized plasmon transducers obtained by thermal embedding of gold island films on glass, Advanced Materials, 20, 3893-3899.
33. Brolo, A.G., Gordon, R., Leathem, B., Kavanagh, K.L. (2004), Surface plasmon sensor based on the enhanced light transmission through arrays of nanoholes in gold films, Langmuir, 20 (12), 4813–4815.
34. Sepúlveda, B., Angelomé, P.C., Lechuga, L.M., Liz-Marzán, L.M. (2009), LSPR-based nanobiosensors, Nano Today, 4(3), 244-251.
35. Abu Hatab, N.A., Oran, J.M., Sepaniak, M.J. (2008), Surface-enhanced Raman spectroscopy substrates created via electron beam lithography and nanotransfer printing, ACS Nano, 2 (2), 377–385.
36. Tsargorodska, A., El Zubir, O., Darroch, B., Cartron, M. L., Basova, T., Hunter, C. N., Nabok, A., Leggett, G. J. (2014), Fast, simple, combinatorial routes to the fabrication of reusable, plasmonically active gold nanostructures by interferometric lithography of self-assembled monolayers, ACS Nano, 8 (8), 7858–7869.
37. Haynes, C.L., Van Duyne R.P. (2001), Nanosphere Lithography: A Versatile Nanofabrication Tool for Studies of Size-Dependent Nanoparticle Optics, J. Phys. Chem. B, 105 (24), 5599–5611.
38. Townsend, E., Bryant, G.W. (2012), Plasmonic properties of metallic nanoparticles: The effect of size quantization, Nano Letters, 12, 429-434.

39. Tame, M.S., McEnery, K.R., Özdemir, Ş.K., Lee, J., Maier, S.A., Kim, M.S. (2013), Quantum plasmonics, Nature Physics, 9, 329–340.
40. Petryayeva, E., Krull, U.J. (2011), Localized surface plasmon resonance: nanostructures, bioassays and biosensing – A review, Analytica Chimica Acta, 706, 8-24.
41. Mayer, K.M., Hafner, J.H. (2011), Localized surface plasmon resonance sensors, Chemical Reviews, ACS, 111, 3828-3857.
42. Hutter, E., Fendler, J.H. (2004), Exploitation of localized surface plasmon resonance, Advanced Materials, 16(19), 1685-1706.
43. Kedem, O., Vaskevich A., Rubinstein, I. (2014), Critical issues in localized plasmon sensing, J. Phys. Chem. C, 118 (16), 8227–8244.
44. Armstrong, R.E., Zijstra, P., Single protein plasmonic sensors using DNA aptamers, XIV Conference on Optical Chemical Sensors and Biosensors, Europt(r)ode XIV, March 25-28, 2018, Naples, Italy, OC14.
45. Tesler, A.B., Maoz, B.M., Feldman,Y., Vaskevich, A., Rubinstein, I. (2013), Solid-state thermal dewetting of just-percolated gold films evaporated on glass: development of the morphology and optical properties, J Phys. Chem.,117, 11337-11346.
46. Al Rubaye, A.G., Nabok, A., Tsargorodska, A. (2017), Spectroscopic ellipsometry study of gold nanostructures for LSPR bio-sensing applications, Sensing & Bio-Sensing Research, 12, 30–35.
47. Al-Rubaye, A.G., Nabok, A., Abu-Ali, H., Szekacs, A., Takacs E., LSPR/TIRE bio-sensing platform for detection of low molecular weight toxins, IEEE Sensors, 29 Oct. - 1 Nov., 2017, Glasgow, UK, https://ieeexplore.ieee.org/abstract/document/8234116/.
48. Al-Rubaye, A.G., Nabok, A., Tsargorodska, A. (2016), LSRP biosensor based on nano-structured gold films: Detection of mycotoxins, 26th Anniversary World Congress on Biosensors, Gothenburg, Sweden, 25-27 May, 2016, Procedia Technology, 27, 131-132.
49. Al-Rubaye, A., Nabok, A., Abu-Ali, H., Szekacs, A., Takacs, E. (2017), LSPR/TIRE bio-sensing platform for detection of low molecular weight toxins, IEEE Sensors, Glasgow, 29 Oct.-1 Nov. 2017, DOI: 10.1109/ICSENS.2017.8234116
50. Al Rubaye, A.G., Nabok, A., Catanante, G., Marty, J.-L., Takacs, E., Szekacs, A. (2018) Optical aptamer biosensors based on gold nanostructures for detection of mycotoxins, Toxins (in press).
51. Nabok, A. (2016), Comparative studies on optical biosensors for detection of bio-toxins, in Advanced Sciences and Technologies in Security Applications, Biosensors for Security and Bioterrorism Applications, Eds. D.P. Nikolelis and G.P. Nikoleli, Springer, 2016, 491-508.
52. Lechuga, L.M. (2005), Optical biosensors, Comprehensive Analytical Chemistry, 44, 209-250.
53. Berney, H., Oliver, K. (2005) Dual polarization interferometry size and density characterisation of DNA immobilisation and hybridisation, Biosensors and Bioelectronics, 21, 618–626.
54. Escorihuela, J., González-Martínez, M.Á., López-Paz, J.L., Puchades, R., Maquieira, Á., Gimenez-Romero, D. (2015) Dual-polarization interferometry: a novel technique to light up the nanomolecular world, Chem. Rev., 115 (1), 265–294.
55. Sun, Y., Fan, X. (2011), Optical ring resonators for biochemical and chemical sensing, Analytical and bioanalytical chemistry, Springer, 399(1), 205–211.
56. Kozma, P., Kehl, F., Ehrentreich-Förster E., Stamm, C., Bier, F.F. (2014), Integrated planar optical waveguide interferometer biosensors: A comparative review, Biosensors & Bioelectronics, 58, 287–307
57. K.E. Zinoviev, A.B. González-Guerrero, C. Domínguez, Lechuga, L.M. (2011), Integrated bimodal waveguide interferometric biosensor for label-free analysis, J. Lightwave Technol., 29 (13), 1926-1930.
58. Gavela, A.F., García, D.G., Ramirez, J.C., Lechuga, L.M. (2016), Last advances in silicon-based optical biosensors, Sensors 16, 285–300.
59. Misiakos, K., Petrou, P.S., Kakabakos, S.E. , Yannoukakos, D., Contopanagos, H., Knoll, T., Velten, T., De Fazio, M., Schiavo, L., Passamano, M., Stamou, D. Nounesis, G. (2010), Fully integrated monolithic optoelectronic transducer for real-time protein and DNA detection. The NEMOSLAB approach, Biosensors and Bioelectronics, 26, 1528–1535.
60. K. Misiakos, (2011), Monolithic silicon optocouplers for bio-chemical sensing, Proceedings of Eurosensors XXV, 25, 152–155.
61. Shirshov, Y.M., Snopok, B.A., Samoylov, A.V. , Kiyanovskij, A.P., Venger, E.F., Nabok, A.V., Ray, A.K. (2001), Analysis of the response of planar interferometer to molecular layer formation: fibrinogen adsorption on silicon nitride surface, Biosensors & Bioelectronics, 16, 381–390.

62. Nabok, A., Starodub, N.F., Ray, A.K., Hassan, A.K., Registration of immuno-globuline AB/AG reaction with planar polarization interferometer, Proceedings of SPIE, Biochemical and Biomolecular Sensing, Environmental and Industrial Sensing, Photonics East, Boston US, 5–8 Nov., 2000, 4200–4201.
63. Nabok, A.V., Haron, S.A., Ray, K. (2004), Optical enzyme sensors based upon silicon planar waveguide coated with composite polyelectrolyte film, Applied Surface Science, 238, 423–428.
64. Nabok, A., Al-Jawdah, A.M., Tsargorodska, A. (2017), Development of planar waveguide-based immunosensor for detection of low molecular weight molecules such as mycotoxins, Sensors & Actuators B: Chemical, 247, 975–980.
65. Al-Jawdah, A., Nabok, A., Al-Rubaye, A., Holloway, A., Tsargorodska, A., Takacs, E. , Szekacs, A. (2018) Mycotoxin biosensor based on optical planar waveguide, Toxins, (in press).
66. Al-Jawdah, A., Nabok, A., Abu-Ali, H., Catanante, G., Marty, J-L., Szekacs, A. (2018) Highly sensitive label-free detection of aflatoxin B1 in aptamer assay using optical planar waveguide operating as polarization interferometer, 28 Anniversary World Congress on Biosensors, 12-15 June, 2018, Miami, FI, US (submitted to Biosensors and Bioelectronics).